Journal of Alloys and Compounds 522 (2012) 90–95

Contents lists available at SciVerse ScienceDirect

Journal of Alloys and Compounds

journal homepage: www.elsevier.com/locate/jallcom

Room temperature relaxor ferroelectricity and spin glass behavior in Sr_2FeTiO_6 double perovskite

P. Neenu Lekshmi [a], S. Savitha Pillai [a], K.G. Suresh [b], P.N. Santhosh [c], Manoj Raama Varma [a,*]

[a] Materials Science and Technology Division, National Institute for Interdisciplinary Science and Technology [NIIST], CSIR, Trivandrum 695 019, India
[b] Department of Physics, Indian Institute of Technology Bombay, Mumbai 400 076, India
[c] Department of Physics, Indian Institute of Technology Madras, Chennai 600 036, India

ARTICLE INFO

Article history:
Received 29 September 2011
Received in revised form 16 January 2012
Accepted 16 January 2012
Available online 2 February 2012

Keywords:
Disordered systems
Crystal structure
Dielectric response
Spin glasses

ABSTRACT

The structure, dielectric and magnetic properties of complex Sr_2FeTiO_6 double perovskite have been investigated. Reitveld analysis of X-ray powder diffraction pattern reveals that the material is stabilized in a cubic perovskite phase with $Pm\bar{3}m$ space group without the B-site cations ordering. The temperature evolution of crystal structural studies indicates the absence of structural changes with temperature. The scanning electron micrograph exhibits heterogeneous grain distribution with average grain size of 1–7.5 μm. The bond valence sum calculations and diffusion-assisted small-polaron hopping conduction mechanism confirm the mixed valence state of Fe/Ti ions. Dielectric spectra show a broad dielectric anomaly coupled with a shift in dielectric maxima towards higher temperature with frequency, exhibiting a typical relaxor ferroelectric behavior. The relaxor behavior has been quantitatively characterized based on the phenomenological parameters (T_m, T_B, γ, ΔT_{relax}). The agreement of dielectric relaxation with non-linear Vogel Fulcher relation indicates that the system is indeed a relaxor exhibiting glassy characteristics. The transport studies show a semiconductor like behavior and a negligible magnetoresistance. Furthermore, the magnetic characterisation exhibits a non-metallic spin-glass-like state below 16 K, driven by competing interactions between the antiferromagnetic and the ferromagnetic states.

1. Introduction

Perovskites present an incredible extensive array of structures and phases with entirely different properties. These materials found wide applications in modern electronic devices such as capacitors, piezoelectric and pyroelectric transducers, resonators, etc. Among the ternary perovskites, the double perovskites of composition $A_2B'B''O_6$ (A – alkaline earth metals such as Ca, Ba, Sr, etc., or rare earth ions of larger ionic radii, B′ and B″ – transition metal cations or lanthanides with smaller ionic radii) have received significant attention in recent years due to their unique electrical and magnetic properties. For instance, some of them exhibit interesting magnetic properties which involves half-metallic ferromagnetic Sr_2FeMoO_6, T_C = 410 K and antiferromagnetic insulator Sr_2FeWO_6, T_N = 37 K [1,2]. Moreover, they exhibit a number of interesting phenomena, including room temperature magnetoresistance, magneto capacitance and magnetostriction. For example, Sr_2FeMoO_6 shows appreciable room temperature tunnelling magnetoresistance ~10% for 7 T magnetic field. The presence of magneto-electric coupling (ME) in these compounds promises important applications in spintronics devices such as magnetic tunnel junctions or low field magnetoresistive sensors [3]. In addition to their magnetic properties, the giant dielectric constant and the dielectric relaxation are also observed, which have generated considerable interest due to their possible applications in technologies like memory storage devices, micro-electro-mechanical system, multilayer ceramic capacitors and optoelectronic devices [4–7].

Recently multiferroic double perovskites such as La_2NiMnO_6, La_2CoMnO_6, Sr_2MMnO_6 (M = Sb^{5+}, Ti^{4+}, Nb^{5+}, W^{6+}, Mo^{6+}, Ta^{5+}), etc. are reported to show near room temperature magneto dielectric effect or magnetocapacitance and subsequent potential applications in spintronics devices such as magneto dielectric capacitors and spin filtering tunnel junctions [8–11]. Additionally, multiferroics are also used in highly sensitive actuators and sensors, multi state memories, robotics, etc. [12,13]. An extensive research has been conducted in a number of Fe containing complex perovskites, $A(Fe_{1/2}B_{1/2})O_3$ (A = Ba, Ca, Sr; B = Nb, Ta, Sb) [14–17] because of their giant dielectric constant, similar to that in $CaCu_3Ti_4O_{12}$ [18,19], with unique dielectric relaxation behavior. The relaxor behavior in complex double perovskites is due to the defect in ordering and there is no structural phase transition as in normal ferroelectrics [20,21]. Moreover, Fe containing double perovskites has attracted

* Corresponding author at: Materials Science and Technology Division, National Institute for Interdisciplinary Science and Technology [NIIST], CSIR, Trivandrum 695 019, Kerala, India. Tel.: +91 471 2515377; fax: +91 471 2491712.
E-mail address: manojraamavarma@yahoo.co.uk (M.R. Varma).

0925-8388/$ – see front matter © 2012 Elsevier B.V. All rights reserved.
doi:10.1016/j.jallcom.2012.01.091

much scientific interest for their magnetic and magneto transport properties. It has been proposed that certain complex perovskite ferroelectric compounds $A(B'_{1/2}B''_{1/2})O_3$ containing transition metal as one of the B-site cations, exhibit magnetic ordering through indirect exchange mechanism [22,23]. Thus the presence of magnetic Fe in octahedral B′ site of $A(B'_{1/2}B''_{1/2})O_3$ perovskite lattice may generate an interesting multiferroic material.

The compound Sr_2FeTiO_6 is a solid solution oxide mixture of ferroelectric $SrTiO_3$ and ferromagnetic $SrFeO_3$. $SrTiO_3$ is a technologically important material and there are various reports on the effect of impurity doping on the properties of this system. The substitution of titanium for iron is of interest because of the stability and site preference of Ti^{4+}. Fe doped $SrTiO_3$ generates highly disordered system which creates giant dielectric response and diffuse dielectric anomaly [24–26]. A systematic evaluation of the magneto-electrical properties in $Sr(Fe_{1/2}Ti_{1/2})O_3$ has not been extensively done and reported yet to the best of our knowledge. Furthermore, the recent theoretical report on the electronic band structure calculations by full-potential augmented plane wave method reveal that Sr_2FeTiO_6 is a magnetic half metal with total magnetic moment ~2 μ_B [27]. The band structure of Sr_2FeTiO_6 consists of spin densities of states with the positive spin projection is completely occupied and has a forbidden gap, while for the band with the negative spin projection, its upper vacant edge starts to be filled at increased valence electron concentrations. Thus, the spectrum is of a metallic type for one spin subsystem (carrier density at the Fermi level is $N\uparrow(E_F) > 0$), but contains a forbidden gap for the opposite spin projection ($N\downarrow(E_F) = 0$), leads to spin polarized half metallic state. The present investigation focuses on the detailed characterisation of the structure, electrical and magnetic properties of Sr_2FeTiO_6 complex double perovskite.

2. Experimental

Polycrystalline powder sample of Sr_2FeTiO_6 was synthesised by conventional solid-state reaction method. Stoichiometric proportion of high purity $SrCO_3$, Fe_2O_3 and TiO_2 (Sigma Aldrich 99.9%) were mixed and preheated at 1273 K for 12 h. The preheated powder was ground thoroughly and calcined at 1473 K for several times with intermediate grinding. The calcined powder was then pressed into pellets and sintered at 1673 K for 12 h in ambient atmosphere to obtain maximum density. The phase identification and purity of the powder sample was checked from powder X-ray diffraction pattern obtained with a PANalytical X' pert Pro diffractometer in Bragg-Brentano geometry with Cu-Kα radiation in the 2θ range of 10°–90° with a step size of 0.008° at 25 s per scan speed of 0.05°/min. For the temperature dependent structural analysis, a reflective XRD apparatus equipped with a closed cycle helium refrigerator was employed. Rietveld refinement of the diffraction pattern was carried out using the GSAS software. The following parameters were refined: background points, zero shift, unit-cell parameters and thermal effects. The microstructure and grain size of the sintered pellets were observed by scanning electron micrograph using JEOL 5600 LV scanning electron microscope (SEM) at 15 kV. SEM images recorded were analysed using image analysis software (Leica Qwin). Dielectric measurements were carried out on a disc shaped pellet with silver paste electrodes painted on to it. The dielectric permittivity data in the frequency range 10 Hz to 1 MHz and temperature range 223–323 K were recorded using Solartron, SI 1260, impedance analyzer with an ac field amplitude of 100 mV. The magnetization experiments were performed in a vibrating sample magnetometer attached to a physical property measurement system (PPMS-Quantum Design).

3. Results and discussion

3.1. Structural and microstructural study

The room temperature powder X-ray diffraction pattern of polycrystalline Sr_2FeTiO_6 reveals a single phase cubic structure without any superstructure reflections (odd Miller indices, *hkl*), which indicates the absence of long-range Fe/Ti ions ordering in this compound [28,29]. The measure of the stability/mismatch of

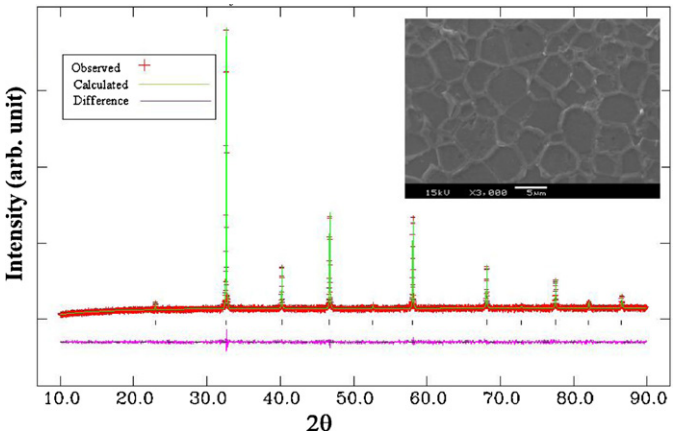

Fig. 1. Observed, calculated and difference X-ray powder diffraction pattern for Sr_2FeTiO_6. The tick marks represent the possible Bragg reflections of Sr_2FeTiO_6. Inset SEM micrograph of Sr_2FeTiO_6 ceramics.

perovskites ABO_3 can be obtained from the tolerance factor (t) by the formula,

$$t = \frac{r_A + r_O}{\sqrt{2}(((r_{B'} + r_{B''})/2) + r_O)}$$

where r_A, $r_{B'}$, $r_{B''}$ and r_O are the ionic radii of the ions [30]. The value of $t = 1$ corresponds to cubic perovskite and if the value is away from 1, it suggests high degree of internal strain due to size mismatch, which lead to a distorted perovskite structure. The value of t is found to be 1.006 for Sr_2FeTiO_6. The Rietveld refined fit of room temperature X-ay diffraction pattern is shown in Fig. 1. As expected the crystal structure of Sr_2FeTiO_6 is cubic and successfully refined in $Pm\bar{3}m$ space group with the lattice parameter, $a = 3.9002(2)$ Å, cell volume 59.33(1) Å^3, R_{wp} factor of 7.31% and R_p of 5.72%. In this structure Sr atoms occupy 1*b* positions, Fe/Ti in 1*a* and the oxygen atoms located at the 3*d* positions. The temperature dependent X-ray diffraction pattern of the sample was also studied. The sequential refinement from 273 K to 298 K was performed with $Pm\bar{3}m$ space group. The thermal evolutions of structural parameters are presented in Table 1, which shows an absence of structural phase transition. The slight decrease in lattice parameter and volume indicate usual contraction of the cubic phase with decreasing temperature.

Bond valence sum (BVS) calculation was done to determine the valence state of Fe and Ti ions. The effective valence V_{ij} between the ith and jth atoms is defined as $V_{ij} = \sum_j e^{((d_0 - d_{ij})/0.37)}$, where d_{ij} is the bond length between i and j atoms and d_0 is the bond valence parameter that has been empirically determined for the i–j pair [31]. Bond valence sum was calculated from Fe—O and Ti—O bond lengths at various temperature using the software SPuDs and is listed in Table 1, which indicate valence fluctuations between $Fe^{4+}/Fe^{3+}$and Ti^{4+}/Ti^{3+} due to the presence of oxygen vacancies [32,33]. As shown by Anderson et al. [29], long range cation ordering in double perovskites stabilizes when there is a significant difference in charge or size of the cations [28]. These differences act as a driving force for the cations to occupy crystallographically distinct positions within the structure. In the case of Sr_2FeTiO_6, the lack of long range cation ordering is attributed to the small difference in charges and size of Fe and Ti ions (ionic radius of Fe^{3+}, $r_{Fe^{3+}} = 0.645$ Å; Fe^{4+}, $r_{Fe^{4+}} = 0.585$ Å and Ti^{3+}, $r_{Ti^{3+}} = 0.67$ Å; Ti^{4+}, $r_{Ti^{4+}} = 0.605$ Å) [34]. Scanning electron micrograph (SEM) for Sr_2FeTiO_6 is shown in the inset of Fig. 1. The SEM micrograph at room temperature exhibits heterogeneous grain distribution with average grain size of 1–7.5 μm and shows a proper compactness of the sintered pellet.

Table 1
Structural parameters, interatomic distances and bond valence sum of Sr_2FeTiO_6 in the cubic space group $Pm\bar{3}m$ at various temperatures.

Temperature (K)	273	278	283	288	293	298
2θ range (°)	10–90	10–90	10–90	10–90	10–90	10–90
Cell parameters, a (Å)	3.89939(1)	3.89954(1)	3.89975(1)	3.89988(1)	3.90005(1)	3.9002(2)
Volume (Å^3)	59.291(0)	59.298(1)	59.308(1)	59.314(1)	59.321(1)	59.33(1)
R_{wp}	0.0567	0.0742	0.0715	0.0710	0.0744	0.0731
R_p	0.0449	0.0588	0.0558	0.0557	0.0585	0.0572
Distances (Å)						
Fe—O	1.94970 (0)	1.94977 (1)	1.94988 (1)	1.94994 (1)	1.95003 (1)	1.95012 (13)
Ti—O	1.94970 (0)	1.94977 (1)	1.94988 (1)	1.94994 (1)	1.95003 (1)	1.95012 (13)
Bond valence sum						
Fe^{3+}	3.59	3.59	3.58	3.58	3.58	3.58
Fe^{4+}	3.75	3.75	3.75	3.74	3.74	3.74
Ti^{3+}	3.91	3.91	3.91	3.90	3.90	3.90
Ti^{4+}	4.17	4.17	4.17	4.17	4.16	4.16

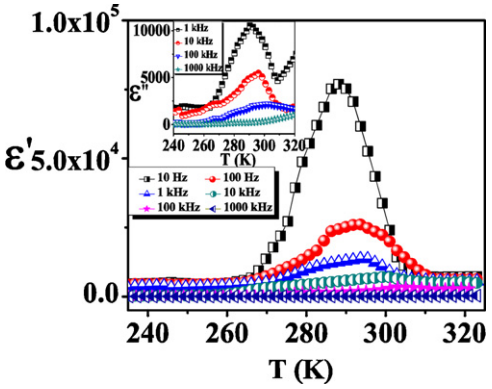

Fig. 2. Real part (ε') of the dielectric permittivity of Sr_2FeTiO_6 as a function of temperature at several frequencies. Inset imaginary part (ε'') as a function of temperature at frequencies 1, 10, 100 and 1000 kHz.

3.2. Dielectric properties

The temperature dependence of the real part ε' and the imaginary part ε'' of dielectric permittivity at several frequencies for Sr_2FeTiO_6 are shown in Fig. 2 and in the inset of Fig. 2 respectively. The dielectric constant goes through a broad maximum, which indicates a diffuse phase transition [20,35,36]. The peak temperature (T_m) at which maximum dielectric constant occurs is found to be frequency-dependent and shifts to higher temperatures with increasing frequency. Also, the maximum value of dielectric constant (ε'_m) decreases with increase in frequency. The magnitudes of ε'_m with respective T_m at representative frequencies are as shown in Table 2. The occurrence of a diffuse transition with frequency dispersion of T_m is the characteristic property of relaxor ferroelectrics; furthermore, the analysis of temperature dependent X-ray diffraction pattern confirms the absence of structural transition. The frequency dependent variation of ε' and ε'' at different temperatures are also shown in Fig. 3. The broad peak in the imaginary part of the dielectric permittivity and coincidence of maximum of ε'' with the inflexion point of ε' further evidence the relaxor behavior of the sample [37]. It is known that the relaxor behavior arises due to the composition fluctuation resulting from cation disorder caused by ions of different valency located on crystallographically equivalent sites or due to the presence of thermally activated nano polar domain structure from the symmetry breaking defects. The symmetry breaking defects can be of different origins, such as point defects and intermediate scale ordering of octahedral cations with different radii and charge [37–40].

Table 2
Frequencies, respective dielectric maxima (ε'_m) and peak temperature (T_m) of Sr_2FeTiO_6.

Frequency (Hz)	ε'_m	T_m (K)
10	76,956	287
100	26,080	291
1000	13,649	294
10,000	6971	399
100,000	3460	304
1,000,000	360	323

The presence of relaxor behavior further analysed by the Curie–Weiss law fit. It is well known that the dielectric permittivity of a normal ferroelectric above Curie temperature follows the Curie–Weiss law,

$$\varepsilon' = \frac{C}{(T - T_0)} (T > T_0) \quad (1)$$

where T_0 is the Curie–Weiss temperature and C is the Curie–Weiss constant. Fig. 4 shows the reciprocal of the dielectric constant ($1/\varepsilon'$) versus temperature at 100 Hz for Sr_2FeTiO_6 and its fit to the experimental data by Curie–Weiss law. A deviation from Curie–Weiss law can be clearly seen. The reciprocal dielectric constant starts to follow the Curie–Weiss law above 306 K, defined as Burn temperature (T_B). The difference between T_B and T_m (306 K – 291 K = 15 K) shows a characteristic diffuseness of phase transition [41].

The relaxor ferroelectric behavior of the sample can also be evaluated using a modified Curie–Weiss law [42,43], Eq. (2), which explains the dielectric behavior of the complex ferroelectrics with

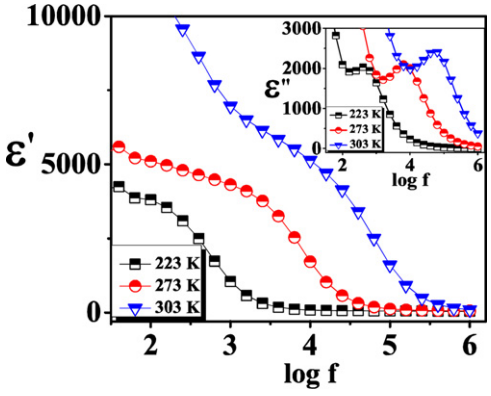

Fig. 3. Real part (ε') of the dielectric permittivity of Sr_2FeTiO_6 as a function of frequency at 223, 273 and 303 K. Inset variation of imaginary part (ε'') with frequency.

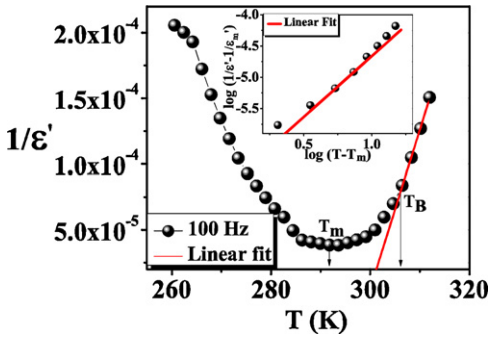

Fig. 4. Temperature variation of the reciprocal dielectric constant $(1/\varepsilon')$ for Sr_2FeTiO_6 fitted with Curie–Weiss law at100 Hz. Inset $\log(1/\varepsilon' - 1/\varepsilon'_m)$ as function of $\log(T - T_m)$ at100 Hz.

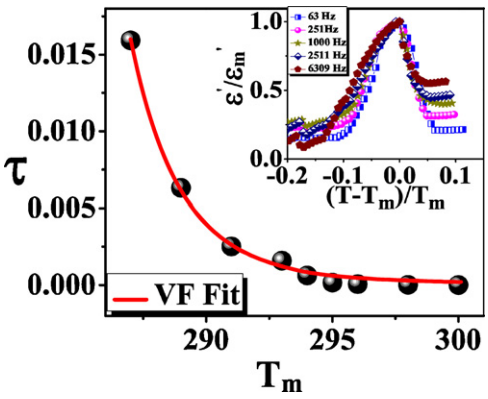

Fig. 5. Non linear Vogel Fulcher fitting for Sr_2FeTiO_6. Inset reduced dielectric permittivity, $\varepsilon'/\varepsilon'_m$, versus reduced temperature, $(T - T_m)/T_m$.

diffuse phase transition, in the temperature range between T_m and T_B,

$$\frac{1}{\varepsilon'} - \frac{1}{\varepsilon'_m} = \frac{(T - T_m)^\gamma}{C} \quad (2)$$

where ε'_m is the dielectric constant at T_m, C is the Curie–Weiss constant, and γ, the diffuseness exponent, lies between 1 and 2. The parameter γ gives an information on the phase transition character; $\gamma = 1$ represents classical ferroelectric phase transition where normal Curie–Weiss law is followed and $\gamma = 1$–2 gives the quadratic dependence which describes completely diffuse phase transition. The plot of $\log(1/\varepsilon' - 1/\varepsilon'_m)$ as a function of $\log(T - T_m)$ at 100 Hz is shown in the inset of Fig. 4. The value of $\gamma \sim 2$ indicates a complete diffuse phase transition characteristics with disordered crystal state of the material [6].

On the other hand, the degree of relaxation behavior can be described by an empirical parameter ΔT_{relax} [41], defined as,

$$\Delta T_{relax} = T_{m(10\,kHz)} - T_{m(10\,Hz)} \quad (3)$$

where $T_{m\,(10\,kHz)}$ and $T_{m\,(10\,Hz)}$ are temperatures corresponding to the maximum dielectric constant at 10 kHz and 10 Hz, respectively and a ΔT_{relax} value of 13 K was observed, which suggests strong frequency dispersion.

The frequency dependent $\varepsilon'(T)$ curve indicates a thermally activated dielectric anomaly since T_m increases with measured frequency. If the dielectric relaxation process is a thermally activated motion, the temperature dependence of the relaxation time can be fitted with Arrhenius law,

$$\tau = \tau_0 \exp\left(\frac{E_a}{k_B T}\right) \quad (4)$$

where τ_0, the pre-exponential term; E_a, activation energy; T, the temperature and k_B, the Boltzmann constant. However, the non linearity in the Arrhenius plots [$\ln(\tau)$ vs. $1000/T$] and the extremely low value of the pre-exponential term τ_0 (1×10^{-77}) indicates failure in fitting the data with Arrhenius law. Therefore, the dielectric spectra for Sr_2FeTiO_6 were fitted with an alternative non-linear Vogel Fulcher (VF) law [43–45],

$$\tau = \tau_0 \exp\left(\frac{E_a}{k_B(T_m - T_f)}\right) \quad (5)$$

which is used to characterize the frequency dispersion behavior in relaxors, where τ_0 is the pre exponential factor; E_a is the activation energy; k_B is the Boltzmann constant; T_m is the temperature at which maximum of ε' occurs at the angular frequency $\omega = 2\pi\nu$; $\tau = \omega^{-1}$ and T_f is the static freezing temperature at which the relaxation time τ tends to infinity. The best fit of VF law to the experimental data indicates that Sr_2FeTiO_6 shows a glassy behavior analogous to the spin glass state in magnetic materials with polarisation fluctuations above T_f. The glassy behavior is attributed to the interaction of random dipoles arising from B-site cations disorder [45–47]. The parameters obtained from the non linear fit (Fig. 5) are $E_a = 0.05$ eV, $\tau_0 = 1.22$ ns and $T_f = 254$ K. The determined parameters are in good agreement with typical values reported for relaxors such as $Pb(Fe_{1/2}Nb_{1/2})O_3$ ($E_a = 0.075$ eV, $\tau_0 = 4.55 \times 10^{-13}$ s, $T_f = 280$ K) [46], $Pb(Ba_{1/3}Nb_{2/3})O_3$ ($E_a = 0.037$ eV, $\tau_0 = 6.66 \times 10^{-6}$ s and $T_f = 286$ K) [47], $FeTiTaO_6$ ($E_a = 0.068$ eV, $\tau_0 = 1 \times 10^{-9}$ s and $T_f = 508$ K) [48], etc.

The broadening of the phase transition is better illustrated by plotting the reduced dielectric constant $(\varepsilon'/\varepsilon'_m)$ as a function of reduced temperature $(\tau = (T_m - T_f)/T_m)$ at different frequencies (inset of Fig. 5). The plot has only a very little dispersion over a wide frequency range similar to the observation in other relaxors [49,50], confirming the ferroelectric relaxor nature of Sr_2FeTiO_6.

The observed relaxation dynamics of Sr_2FeTiO_6 can be attributed to the presence of polar nano regions arising from the compositional fluctuations and/or due to structural disorder in the lattice creating a defect related hopping mechanism [38–40]. This may be correlated with the prevailing disorder at B-site due to the random distribution of the Ti and Fe ions. Furthermore, the presence of mixed valence state, such as Ti^{4+}/Ti^{3+} and Fe^{4+}/Fe^{3+}, also generates a short-range hopping, resulting in dielectric relaxation [24,25,32].

3.3. Transport properties

3.3.1. DC conductivity

Fig. 6 shows the temperature dependence of dc resistivity (ρ_{dc}) measured in the temperature range 150–300 K ($\rho_{dc} \sim 448\ \Omega$ cm at 300 K). In general, any chemical substitution leads to disorder in the system which may tend to localize the carriers at the doping site which are governed by different conduction mechanisms. To analyze the nature of transport behavior, the conductivity data was modelled with common conduction mechanisms such as Arrhenius, variable range hopping and small-polaron hopping models [51]. The conductivity data of Sr_2FeTiO_6 is found to fit well to Mott-small-polaron hopping model.

The diffusion-assisted small-polaron hopping states that,

$$\sigma_{dc} = h_p \left(\frac{N}{a^3}\right) e\mu \ \exp\left(-\frac{E_\mu}{k_B T}\right) \quad (6)$$

In this function, h_p is the hopping probability, N is the number of carriers, a is the average hopping distance, e is the charge of an electron, k_B is the Boltzmann constant, and E_μ is the activation

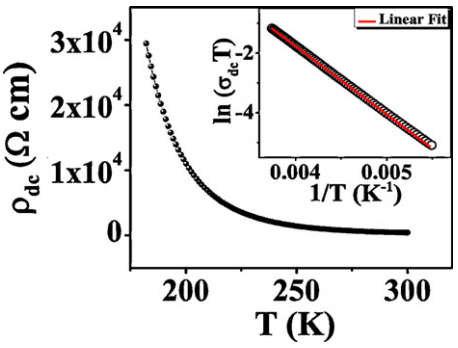

Fig. 6. Temperature dependence of dc resistivity (ρ_{dc}) for Sr_2FeTiO_6. Inset the linear fit with Mott small polaron hopping model.

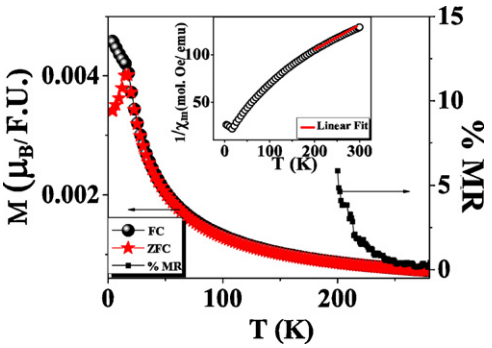

Fig. 8. ZFC and FC magnetization curves for Sr_2FeTiO_6 recorded from 3 K to 300 K at an applied field of 0.5 kOe along with the variation of magnetoresistance with temperature for Sr_2FeTiO_6 at 50 kOe. Inset variation of inverse susceptibility with temperature and the Curie–Weiss fit.

energy for mobility, $\mu = ea^2(\upsilon/kT)$, where υ is the hopping frequency. The plot of $\ln(\sigma_{dc}T)$ as a function of $1/T$ is shown in the inset of Fig. 7. Assuming that hopping occurs between Fe and Ti sites are indistinguishable, one can take the average single-perovskite-type cell parameter $a_l = 3.9002$ Å at 298 K to be the average hopping distance a and hopping probability, $h_p = 1/6$ for the octahedral site for Sr_2FeTiO_6. The value of activation energy and υN extracted from the slope of the linear fit are 0.1941 eV and 1.74×10^{19} Hz respectively. The values are quite typical for semiconductor like carriers. The diffusion-assisted small-polaron hopping conduction in Sr_2FeTiO_6 also indicates an intermediate-valence state of the system [52].

3.3.2. AC conductivity

Fig. 7 shows the ac conductivity (σ_{ac}) as a function of temperature from 250 to 350 K at different frequencies (5, 10, 50 and 100 kHz). The ac conductivity shows a kink around the ferroelectric to paraelectric phase transition which is shifted to the higher temperature side with an increase in frequency and resemble with the shift in dielectric spectra, attributing to the conventional relaxor nature in Sr_2FeTiO_6. This relaxation process associated with the domain reorientation, domain wall motion and the dipolar behavior [53]. At higher temperatures, the conductivity data tends to fall on to a straight line, which is the typical behavior of the dc component [54,55]. The increase in conductivity with increasing frequency suggests that the conduction mechanism is due to the hopping of charge carriers from one site to the other [53].

3.4. Magnetic characterisation

The temperature dependence of zero field-cooled (ZFC) and field-cooled (FC) magnetization for Sr_2FeTiO_6 measured at 0.5 kOe are shown in Fig. 8. The M–T curve exhibits a large thermal irreversibility in the ZFC and FC data below 16 K, suggesting that the material on cooling shows a spin-glass like behavior [33,56]. Battle et al. reported a similar behavior in Sr_2FeRuO_6 due to competing magnetic interactions such as ferromagnetic Fe–Ru superexchange interaction and antiferromagnetic Fe–Fe/Ru–Ru coupling [57]. Plots of inverse susceptibility versus temperature are not linear, indicating that the material does not follow the classical Curie–Weiss law over the whole temperature range which could be arising from the disorder and vacancies in Sr_2FeTiO_6 associated with the complex distribution of Fe exchange paths [55]. However, from the reciprocal of susceptibility in the temperature interval 200–300 K (inset of Fig. 8), an effective magnetic moment, $\mu_{eff} \sim 5.8\ \mu_B$, could be calculated. The effective magnetic moment observed is higher than the theoretical spin only magnetic moment of Fe^{4+}, ($\mu_{(spin)} \sim 4.89\ \mu_B$), Ti^{3+} ($\mu_{(spin)} \sim 1.73\ \mu_B$) and lower than that of Fe^{3+} state ($\mu_{(spin)} \sim 5.92\ \mu_B$). This reveals the presence of mixed oxidation states of Fe and Ti ions arising from the cation disordered structure with random oxygen vacancies [32].

Field dependent magnetisation measurements, performed at temperatures 300 K and 4 K are shown in Fig. 9. M vs. H plot at 300 K reveals a linear behavior, indicating the paramagnetic nature of the material. The field dependent magnetization at 4 K shows a S-shaped hysteresis loop with coercivity (H_c) and remanence (M_r) values as 1.03 kOe and 0.125 emu/g respectively (inset Fig. 9). Furthermore, the magnetization does not saturate even under 50 kOe field, suggesting a spin glass-like behavior of the sample [58]. The observed small moment is only associated with the magnetic state adopted below 16 K owing to the existence of weak ferromagnetic interactions. These interactions usually exist when there is an incomplete antiferromagnetic ordering due to some degree of disorder introduced by the presence of Fe^{4+}, Fe^{3+}, and Ti^{3+} ions leading to the frustration effects. These arise due to the competing

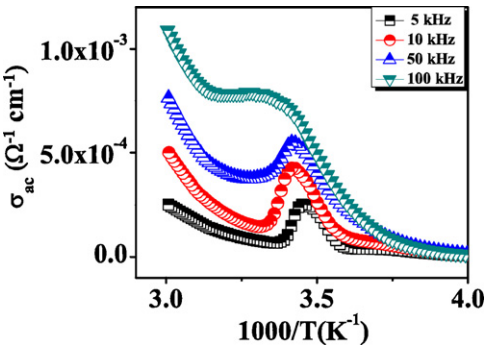

Fig. 7. Temperature dependence of ac conductivity (σ_{ac}) for Sr_2FeTiO_6 at different frequencies.

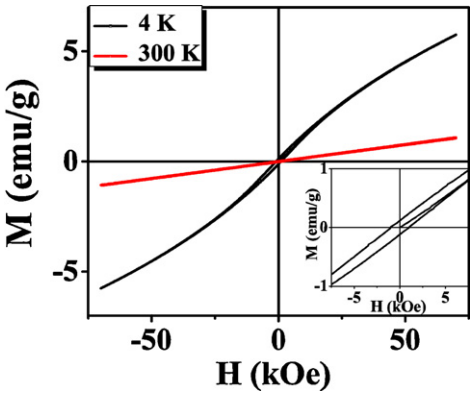

Fig. 9. Magnetisation vs. applied field for Sr_2FeTiO_6 recorded at 4 K and 300 K. Inset shows the expanded region between −7.5 and +7.5 kOe.

ferromagnetic and antiferromagnetic superexchange interactions between Fe ions via Ti/O ions and give rise to spin-glass behavior [26,55]. The magnetoresistance of Sr_2FeTiO_6 was also measured and a negligible value of less than 0.5% for 50 kOe at 300 K was observed (Fig. 8). The low value of magnetoresistance, relaxor ferroelectric nature and spin glass behavior at low temperatures give ample evidence to the conclusion that the localized electronic state arises from the mixed valence state of Fe/Ti ions in this compound [56,59].

4. Conclusions

The structural, dielectric, magnetic and magnetotransport studies of solid state synthesised Sr_2FeTiO_6 double perovskite have been carried out. The Reitveld refinement of X-ray diffraction data reveal the space group of Sr_2FeTiO_6 is $Pm\bar{3}m$ with lattice parameter $a = 3.9002(2)$ Å. The thermal evolution of the lattice parameter and volume shows no structural phase transition and the bond valence sum method reveal the presence of valence fluctuation between $Fe^{4+}/Fe^{3+}$and Ti^{4+}/Ti^{3+}. The microstructure and grain size distribution studied by scanning electron micrograph exhibits heterogeneous grain distribution with average grain size of 1–7.5 μm. The $\varepsilon'(T)$ and $\varepsilon''(T)$ curves show strong frequency dispersion and T_m for lower frequencies are near room temperature, but the temperature dependent X-ray pattern confirms the lack of structural transition, which reveal a typical ferroelectric relaxor behavior. The frequency dependent variations of ε' and ε'' at different temperatures further evidence the presence of short range polar state of the sample. The deviation from Curie–Weiss law and the parameter γ obtained from Modified Curie–Weiss fit, confirm the diffuse phase transition and a relaxor behavior in complex Sr_2FeTiO_6. The degree of relaxation, ΔT_{relax} is obtained as 13 K suggesting strong frequency dispersion and this particular nature indicates that the system freezes to a glassy state below a certain temperature and thereby takes much longer to respond to the small external ac signal. The Vogel–Fulcher relationship indicates a glassy like characteristics and provides another direct evidence of the relaxor behavior in complex Sr_2FeTiO_6 ceramics. The frequency dependence of the real part of ac conductivity at various temperatures also confirms a relaxor ferroelectric behavior. The diffusion-assisted small-polaron hopping conduction in Sr_2FeTiO_6 evidences an intermediate-valence state and semiconductor like behavior of the system. The observed spin-glass like nature of Sr_2FeTiO_6 is attributed to the incompatible superexchange interactions between Fe^{4+}, Fe^{3+}, $Ti^{4+}$and Ti^{3+} ions. These observations suggest, Sr_2FeTiO_6 complex double perovskite is an attractive lead free room temperature relaxor material suitable for practical applications.

Acknowledgments

Manoj Raama Varma and K.G. Suresh acknowledge Department of Science and Technology (DST), India for the financial support. P. Neenu Lekshmi is thankful to Council of Scientific and Industrial Research (CSIR), India for granting the Junior Research Fellowship.

References

[1] K.-I. Kobayashi, T. Kimura, H. Sawada, K. Terakura, Y. Tokura, Nature 395 (1998) 677–680.
[2] H. Kawanaka, I. Hase, S. Toyama, Y. Nishihara, J. Phys. Soc. Jpn. 68 (1999) 2890–2893.
[3] S.A. Wolf, D.D. Awschalom, R.A. Buhrman, J.M. Daughton, S. von Molnar, M.L. Roukes, A.Y. Chtchelkanova, D.M. Treger, Science 294 (2001) 1488–1495.
[4] I.P. Raevski, S.A. Prosandeev, A.S. Bogatin, M.A. Malitskaya, L. Jastrabik, J. Appl. Phys. 93 (2003) 4130–4136.
[5] G.A. Samara, E.L. Venturini, Phase Transitions 79 (2006) 21–40.
[6] I. Rivera, A. Kumar, N. Ortega, R.S. Katiyar, S. Lushnikov, Solid State Commun. 149 (2009) 172–176.
[7] C. Bharti, S.N. Choudhary, T.P. Sinha, J. Surf. Sci. Technol. 24 (2008) 1–10.
[8] M.P. Singh, K.D. Truong, S. Jandl, P. Fournier, Phys. Rev. B 79 (2009) 224421.
[9] K.R.S.P. Meher, M. Savinov, S. Kamba, V. Goian, K.B.R. Varma, J. Appl. Phys. 108 (2010) 094108.
[10] Y.Q. Lin, X.M. Chen, J. Am. Ceram. Soc. 94 (2011) 782–787.
[11] Y.Q. Lin, X.M. Chen, X.Q. Liu, Solid State Commun. 149 (2009) 784–787.
[12] J.F. Scott, Science 315 (2007) 954–959.
[13] N. Ortega, A. Kumar, P. Bhattacharya, S.B. Majumder, R.S. Katiyar, Phys. Rev. B 77 (2008) 01411.
[14] S. Saha, T.P. Sinha, J. Phys.: Condens. Matter 14 (2002) 249–258.
[15] Z. Wang, X.M. Chen, L. Ni, X.Q. Liu, J. Appl. Phys. 90 (2007) 022904.
[16] Y.Y. Liu, X.M. Chen, X.Q. Liu, L. Li, Appl. Phys. Lett. 90 (2007) 192905.
[17] S. Ke, H. Huang, J. Appl. Phys. 108 (2010) 064104.
[18] C.C. Homes, T. Vogt, S.M. Shapiro, S. Wakimoto, A.P. Ramirez, Science 293 (2001) 673–676.
[19] S. Ke, H. Huang, H. Fan, Appl. Phys. Lett. 89 (2006) 182904.
[20] L.E. Cross, Ferroelectrics 76 (1987) 241–267.
[21] G.A. Samara, J. Phys.: Condens. Matter 15 (2003) R367.
[22] L. Mitoseriu, D. Marre, A.S. Siri, P. Nanni, Appl. Phys. Lett. 83 (2003) 5509.
[23] Y. Yang, J.M. Liu, H.B. Huang, W.Q. Zou, P. Bao, Z.G. Liu, Phys. Rev. B 70 (2004) 132101.
[24] C. Ang, J.R. Jurado, Z. Yu, M.T. Colomer, J.R. Frade, J.L. Baptista, Phys. Rev. B 59 (1998) 11858.
[25] C. Ang, Z. Yu, Z. Jing, P. Lunkenheimer, A. Loidl, Phys. Rev. B 61 (2000) 3922.
[26] P. Adler, J. Mater. Chem. 9 (1999) 471–477.
[27] V.V. Bannikov, I.R. Shein, V.L. Kozhevnikov, A.L. Ivanovskii, J. Struct. Chem. 49 (2008) 781–787.
[28] P. Woodward, R.D. Hoffmann, A.W. Sleight, J. Mater. Res. 9 (1994) 2118–2127.
[29] M.T. Anderson, K.B. Greenwood, G.A. Taylor, K.R. Poeppelmeier, Prog. Solid State Chem. 22 (1993) 197–233.
[30] J.B. Philipp, P. Majewski, L. Alff, A. Erb, R. Gross, T. Graf, M.S. Brandt, J. Simon, T. Walther, W. Mader, D. Topwal, D.D. Sarma, Phys. Rev. B 68 (2003) 144431.
[31] I.D. Brown, D. Altermatt, Acta Crystallogr. B 41 (1985) 244–247.
[32] T.C. Gibb, P.D. Battle, S.K. Bollenb, R.J. Whitehead, J. Mater. Chem. 2 (1992) 111–114.
[33] C. Greaves, R.A. Buker, Mater. Res. Bull. 21 (1986) 823–833.
[34] R.D. Shannon, C.T. Prewitt, Acta Crystallogr. B25 (1969) 925–946.
[35] K.N. Singh, P.K. Bajpai, J. Alloys Compd. 509 (2011) 5070–5074.
[36] K.S. Rao, B. Tilak, K.Ch.V. Rajulu, A. Swathi, H. Workineh, J. Alloys Compd. 509 (2011) 7121–7129.
[37] M. Bouziane, A. Benabad, J.C. Niepce, B. Elouadi, J. Electroceram. 23 (2009) 19.
[38] W. Kleemann, J. Mater. Sci. 41 (2006) 129–136.
[39] S.B. Krupanidhi, Proc. Indian Acad. Sci.: Chem. Sci. 115 (2003) 775–788.
[40] L.P. Curecheriua, L. Mitoseriua, A. Ianculescu, J. Alloys Compd. 485 (2009) 1–4.
[41] L. Zhou, P.M. Vilarinho, J.L. Baptista, J. Electroceram. 5 (2000) 191–199.
[42] K. Uchino, S. Nomura, Ferroelectr. Lett. Sect. 44 (1982) 55–61.
[43] G. Fulcher, J. Am. Ceram. Soc. 8 (1925) 339.
[44] J. Zhang, C. Boyd, W. Luo, Phys. Rev. Lett. 2 (1999) 390–393.
[45] R. Pirc, R. Blinc, Phys. Rev. B 76 (2007) 020101.
[46] C. Bharti, S.N. Choudhary, T.P. Sinha, Indian J. Phys. 83 (2009) 409–414.
[47] P.K. Bajpai, M. Pastor, K.N. Singh, J. Appl. Phys. 109 (2011) 014114.
[48] Y. Shi, Y.-D. Hou, C. Wang, H.-Y. Ge, M.-K. Zhu, J. Am. Ceram. Soc. 93 (2010) 2491.
[49] M. Tyunina, J. Levoska, A. Sternberg, S. Leppavuori, J. Appl. Phys. 86 (1999) 5179.
[50] M.R. Panigrahi, S. Panigrahi, J. Electroceram., doi:10.1007/s10832-011-9631-1.
[51] N.F. Mott, Metal-Insulator Transitions, Taylor & Francis, London, 1990.
[52] P.M. Woodward, J. Goldberger, M.W. Stoltzfus, H.W. Eng, R.A. Ricciardo, P.N. Santhosh, P. Karen, A.R. Moodenbaugh, J. Am. Ceram. Soc. 91 (2008) 1796–1806.
[53] B. Behera, E.B. Araujo, R.N. Reis, J.D.S. Guerra, Adv. Condens. Matter Phys., 2009 (Article ID: 361080, 6 pages, doi:10.1155/2009/361080).
[54] C. Karthik, K.B.R. Varma, J. Phys. Chem. Solids 67 (2006) 2437–2441.
[55] D.A. Sanchez, A. Kumar, N. Ortega, R.S. Katiyar, J.F. Scott, Appl. Phys. Lett. 97 (2010) 202910.
[56] L.O.S. Martin, J.P. Chapman, L. Lezama, J.J.S. Garitaonandia, J.S. Marcos, J.R. Fernández, M. Arriortuac, T. Rojo, J. Mater. Chem. 16 (2006) 66–76.
[57] P.D. Battle, T.C. Gibb, C.W. Jones, F. Studer, J. Solid State Chem. 78 (1989) 281–293.
[58] J.G. Booth, J. Crangle, Proc. Phys. Soc. 79 (1962) 1278.
[59] Y.S. Kim, J. Kim, S.J. Moon, W.S. Choi, Y.J. Chang, J.-G. Yoon, J. Yu, J.-S. Chung, T.W. Noh, Appl. Phys. Lett. 94 (2009) 202906.